Nanoscale

Accepted Manuscript

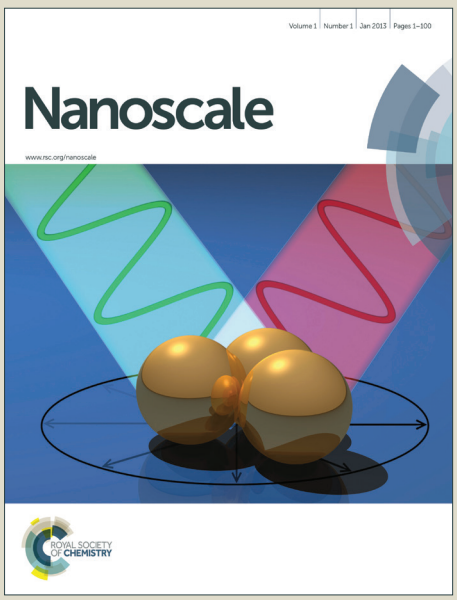

ROYAL SOCIETY OF CHEMISTRY

www.rsc.org/nanoscale

Cite this: DOI: 10.1039/c0xx00000x

www.rsc.org/xxxxxx

COMMUNICATION

Epitaxial Transfer through End-Group Coordination Modulates Odd-Even Effect in Alkanethiol Monolayer Assembly†

Yeneneh Y. Yimer,[‡a] Kshitij C. Jha [‡a] and Mesfin Tsige*[a]

[a] *Department of Polymer Science, The University of Akron, Akron, Ohio 44325, USA, Fax: 330- 972-5290; Tel: 330- 972-5631; E-mail: mtsige@uakron.edu*

[‡] *These authors contributed equally to this work*

**** Corresponding Author; E-mail: mtsige@uakron.edu***

† Electronic Supplementary Information (ESI) available: Models, parameters, metal potentials are discussed and computational details on tilt angle vectors, hydrogen bond networks, adatom profiles and energies, epitaxial transfer, energy per chain and mobility are provided.

Table of Content (TOC)

Novelty: End-functional groups control monolayer assembly through co-ordination with adlayer in *n*-alkanethiol assembly on gold {111}.

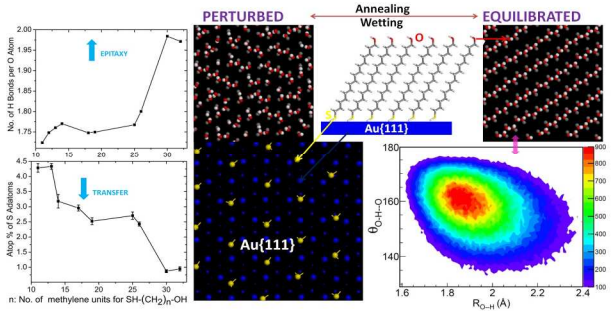

Short spacer length and high end-group coordination lead to the top network acting as a template for the buried sulfur-gold interface of *n*-alkanethiols (SH-$(CH_2)_n$-OH or SH-$(CH_2)_n$-CH_3) on gold {111}. Annealing and templating both drive toward a higher sampling of the spatially favorable bridge adsorption sites. The hydrogen-bonded network increases in strength by increasing the number of hydrogens participating per oxygen, from 1.75 to 1.98 for n=14→30. Higher n leads to better packing (five times for hydroxyl-terminated and seven times for methyl-terminated for n=14→30) and stability of monolayers, while lower n results in better epitaxial transfer (transfer coefficient ratio = 13.5 for {SH-$(CH_2)_{14}$-OH }/{ SH-$(CH_2)_{30}$-CH_3}) and actuation. Odd values of n for the hydroxyl-terminated *n*-alkanethiols lead to lattice spacing an average of 0.04±0.01 Å higher than even values. There is a structural transition in properties around spacer length n=24-27. Characterization of monolayer assembly through correlation between adatom and network layers provides recursive design principles for actuation and sensing applications.

Alkanethiol monolayer assembly on gold is one of the most studied systems for self-assembled monolayers (SAMs).[1,2] It also happens to be perfect for analysis of the effect of van der Waals forces in monolayer assembly,[3,4] a subject that has kindled recent interest in materials science.[4,5] Design tools that exploit van der Waals forces could, for example, lead to utilization of conformational changes for functionality[6-12] in addition to the π-π stacking approaches that have been a traditional focal point.[13] A majority of the analyses of thiol-anchored monolayer self-assembly on gold have focused on the interactions of sulfur or anchoring groups with noble metal surfaces.[14-16] The influence of end-groups and their effect on buried layer epitaxy has been examined experimentally,[17-19] although quantification remains a challenge because of the resolution limitations through microscopy (AFM, STM), and spectroscopy (NEXAFS). Adsorption sites have previously been analyzed through density functional theory and scanning tunneling microscopy.[14,15,20,21] However, a dynamic view of the variation of the adsorption site distribution with temperature and chain length is missing. The need for such a distribution has been recognized towards understanding the local minima and defects as well as the effect of kinetics and thermodynamics on the adatom profile, which remains difficult to characterize.[22,23] We show that the end functional groups are a major contributor to monolayer assembly and drive the packing and adsorption of *n*-alkanethiol monolayers on gold {111}.

We simulated methyl- and hydroxyl-terminated *n*-alkanethiols -- which are representative of two opposite polarities at the top interface often analyzed for anti-corrosion and anti-biofouling applications.[24,25] All-atom Molecular Dynamics on a range of spacer lengths (n = 11-32) using accurate metal potentials[26] for gold and well tested OPLS-AA parameters[27] for *n*-alkanethiols were run for simulation times greater than 5 ns. The metal potentials used have previously predicted adsorption energies and soft epitaxial effects (Supporting Information section S1, for further details on simulation models, parameters, protocols, and metal potentials) at the metal-organic interface in good agreement with experiments.[28,29] The gold layers are not constrained, unlike previous studies, which have simplified analysis with frozen or virtual gold[30,31] that may lead to loss of the dynamic nature of the adatom profile.

Quantification through tilt angle distribution using the S-O and S-C vectors for hydroxyl- and methyl-terminated *n*-alkanethiols provides high resolution morphological information that gives trends unobtainable by standard empirical methods. Figure 1 shows the definition of tilt angle vectors. The average S-C tilt angles for both hydroxyl- and methyl- terminated *n*-alkanethiol monolayers, in our study, showed tilt angles from 32-35^0. This matches the reported range of 25-35^0 observed by Strong and Whitesides[32] using electron diffraction and about 30^0 reported by Cossaro *et al.*[33] using X-ray diffraction and molecular dynamics.

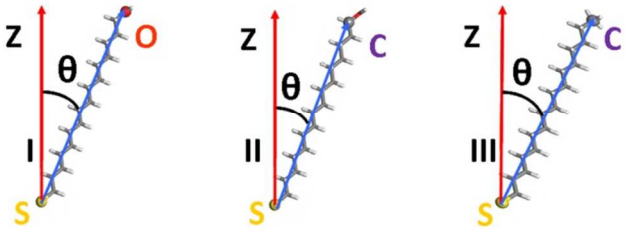

Figure 1. Schematic for definition of the tilt angle θ for different end terminated *n*-alkanethiols. I) S-O tilt angle for hydroxyl terminated, II) S-C tilt angle for hydroxyl terminated. III) Tilt angle for methyl terminated.

Specifically, we observe that the S-O vector for hydroxyl-terminated *n*-alkanethiols exhibits a symmetric split (Figure 2C, 3B, and 4B) with peaks varying sharply with changes in the nature of the network. This provides quantification that is hard to obtain through experiments, as the empirical measurements are along the backbone (or the S-C vector). The tilt angle through the S-O vector is more sensitive to changes in annealing and wetting and was chosen for all analyses in the present paper. Supporting Information Figure S1 shows change in tilt angle distribution with chain length for methyl-terminated *n*-alkanethiols and Figure S2 shows change in S-C tilt angle distribution with temperature for hydroxyl-terminated *n*-alkanethiols. These when taken in conjunction with changes in S-O tilt angle distribution establish the higher sensitivity of the S-O vector as a marker for quantifying structural changes in the monolayer. The mobility of the chains is lowered dramatically above n=14, therefore this was selected as a cut-off point for short-chain assembly, while n=30 is the onset of long-chain assembly as seen through saturation effects and structural transition. The effects of annealing through heating and cooling cycles and wetting by water have also been examined.

The network formed by end-group co-ordination is referred to in our work as the top network, and the transfer to the adatom layer in terms of the top network is considered as a *soft epitaxial effect*. We quantify this effect by defining the correlation between the variance of the radial distribution of the top network O-O (C-C for methyl-terminated as a control without any network) and the

variance of bottom layer S-S (also the adatom layer) with temperature. We call the change in variance *epitaxial transfer* and hypothesize competing interactions from mobility (decreasing with increasing spacer length), and network strength (increasing with increasing chain length) as affecting the transfer. The *epitaxial transfer* can be seen with changes in the population profiles of the adatom layer. This is observed most significantly through decreases in atop percentage, which is a measure of hopping from hollow to bridge sites. We observe a decrease in atop population by 2-2.5% in the transition from short to long chains. This implies increased stability but decreased transfer (low hopping, hence low mobility).

The hydrogen-bonded network lies roughly along parallel lines (Figure 2A and 2B) and exhibits long-range propagation. It is instructive to compare hydroxyl-terminated *n*-alkanethiols possessing a top hydrogen-bonded network to methyl-terminated *n*-alkanethiols with no top network as a control for the observed trends.

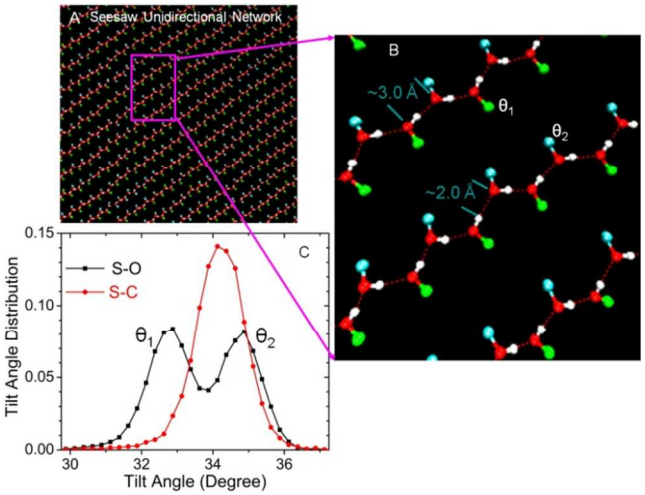

Figure 2: Nature of *unidirectional seesaw* hydrogen-bonded network for hydroxyl-terminated *n*-alkanethiols. Carbons attached to oxygens with lower tilt angle (θ_1) are in green. Carbons attached to oxygens with higher tilt angle (θ_2) are in cyan. Only the hydrogens attached to the oxygens are shown to illustrate the 2-D unidirectional hydrogen-bonded network. Oxygens are in red, and hydrogens are in white. A) A top view snapshot with a unit repeat cell marked and enlarged which is shown in B) where the zigzag hydrogen-bonded network in higher resolution is visible with the distances labeled along with the two angles observed for the split peak when measuring S-O tilt angle distribution. C) Shows the two-peak tilt angle distribution for the S-O vector, which is due to the zigzag network formed. The S-O tilt angle distribution gives a measure of the ordering of the hydrogen-bonded network and is a sensitive quantifier to perturbations of the network. The split peak *saddle* is spread over ~2°. The bin size chosen for the distribution was 0.5° to account for reasonable statistics for visualization of the *saddle*. The maximum error, therefore, in all tilt angle distributions would be half the bin size, or ±0.25°. Bin sizes with lower values were also used to see distribution dependence. *Saddle* spread and the nature of the split peak was independent of bin size for values less than 0.5°.

We also find that distribution plots of distance versus angle (O-H and O-O) for hydrogen bonding identify the extremely narrow distribution of the 2x2 network shown in Figure 2. Supporting Information section S3 has details on hydrogen bond computation and Figure S3 shows distribution plots for distance versus angle for n=30. It also clearly shows the density distribution akin to a Ramachandran plot for a well-formed network, which fits two hydrogen bonds per oxygen atom for the perfectly formed network for long chain lengths (n≥30).

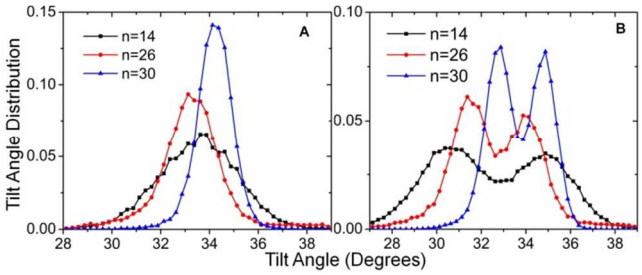

Figure 3: Tilt angle distribution (S-C and S-O) with chain length for hydroxyl-terminated *n*-alkanethiols. A) Increasing chain length for hydroxyl-terminated *n*-alkanethiols leads to a more compact structure, with narrower peaks shown for the S-C tilt angle distribution. B) Increasing chain length produces the same effect on the S-O tilt angle distribution of hydroxyl-terminated *n*-alkanethiols, but with symmetric split peaks.

Network Nature

The morphology of the top network which acts as a template for the buried interface for hydroxyl-terminated thiols, can be seen through the top-view snapshot of the equilibrated trajectory (Figure 2A), and the probability distributions of the S-O tilt angle vectors (Figure 2C). Distances on the zigzag hydrogen-bonded network (Figure 2B), show an average O···H distance of ~2 Å and O–H···O angle of ~157°, consistent with empirical observations for aliphatic alcohols[34] which are within range of the values for classical hydrogen bond using bulk water (Supporting Information Section S3). The nature of this *unidirectional seesaw* hydrogen-bonded network can be read from the distribution plot of distance between participating hydrogen bonds (O···H) and the distance between neighboring oxygens (O---O) versus angle (O-H···O) (Supporting Information Section S3, Figure S3) as well as the visualization of trajectories. The nearest oxygen neighbors are packed at a spacing of ~2.9-3.0 Å (Figure 2B). We observe the spacing of oxygen neighbors for odd chain lengths increasing on average by 0.04±0.01 Å compared to even chain lengths. The differential in odd versus even lattice spacing also increases with increasing chain length (cf. Figure 6B). The number of hydrogens participating per oxygen in the hydrogen-bonded network increases with chain length.

The symmetric S-O tilt angle vector distribution with equal population for the two peaks (Figure 2C, 3B, and 4B) reflects the equilibrated network. Changes in network morphology upon annealing and wetting were characterized through changes in the tilt angle distribution. Better bonded networks can express

themselves both in terms of distortion of the underlying methylene group adjacent to the end functional group which was observed for amide-terminated alkanethiol monolayers[17] or in terms of whole-chain translation seen in the current study. The whole chain translation has been observed through increase in hopping evidenced by increasing transitional atop percentage. Geometrically, the bridge:atop:hollow ratio is 3:2:2 for the gold {111} surface. We found, on average, the hollow binding sites as favored by 0.06±0.01 kcal/mol over the bridge sites, while atop sites are the least favored, being 0.3±0.01 kcal/mol higher in energy when compared to the corresponding hollow sites (Supporting Information section S4, Figure S4 and Tables S1 and S2 for computational details and values of energies and assignment of binding sites). A large number of computational studies, mostly DFT based, have observed that the hollow and bridge sites have increased adsorption affinity compared to the atop binding site.[20] Some STM studies[20] have disputed the current understanding of the atop binding site being least favorable. However, all these studies on the nature of the adlayer have been focused on either quantum mechanical treatments and/or extremely small chain lengths. Through justified metal potentials and a range of chain lengths, we have attempted to understand the dynamic nature of the adlayer taking into account the mobility of the sulfur, 'unfrozen and non-virtual' gold, and the effect of packing. Population profiles match well with the adsorption energy trends which show atop site to be least favorable.

Added energy to an equilibrated system would shift some adsorption sites to the spatially more favorable bridge sites. An increase in the percentage of atop sites by approximately 2- 2.5% for shorter chains and at higher temperatures is an indicator of increased hopping of sulfur. We observe this in terms of spatially favored increased bridge percentage (Supporting Information Section S4 for population analyses, Tables S3 and S4 showing site distribution for hydroxyl- and methyl-terminated *n*-alkanethiols as a function of chain length and temperature, respectively).

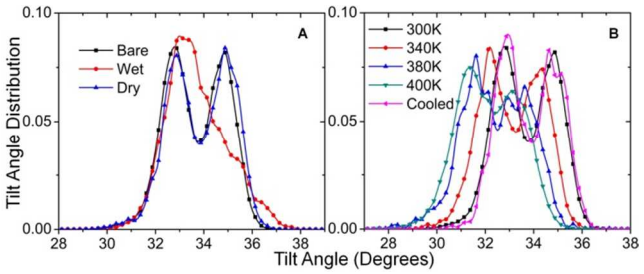

Figure 4: Effect of wetting and annealing on tilt angle distribution for n=30 hydroxyl-terminated *n*-alkanethiols. A) Wetting with water leads to no hysteresis and recovery of the original tilt angle distribution. With water, the ordering is destroyed but the peak does not shift to the left. The interfacial water destroys long- and short-range order in terms of the interfacial hydroxyl groups but keeps the mean distribution around the same value as the non-wetted system. B) Heating and cooling cycles for hydroxyl-terminated *n*-alkanethiols leads to no hysteresis. Upon heating, both the distortion in double peak and a systematic shift to the left of the S-O tilt angle distribution increase with increasing temperature. All tilt angles are from sulfur to oxygen of the hydroxyl end-group. After 400 K, even for a higher chain length system like n=30, the monolayer assembly loses stability and we get a single peak similar to wetted system.

The network nature of a 2x2 seesaw network quantified through tilt angle distribution and the effect of adsorption energies on the population profile are responsible for the modulation of the various properties of the monolayer assembly. Their correlation is examined in the following sections.

Network Modulation

The morphology and local ordering of the top network are reflected in the distribution of the tilt angles. We have shown the variation in S-C and S-O tilt angle distributions with chain lengths for hydroxyl-terminated *n*-alkanethiols in Figure 3. The peak height for both tilt angle distributions increases with chain length. For the S-O tilt angle distribution, in comparison to the S-C tilt angle distribution, of hydroxyl-terminated *n*-alkanethiols, the peak height is lower, and changes in distribution would be magnified, with the break in symmetry of the double peak also serving as a quantifier. Hence, the S-O tilt angle distribution for hydroxyl-terminated *n*-alkanethiols is a more sensitive quantifier of the morphology of the top network and the packing of the monolayer assembly. Calculation of the S-O and S-C tilt angle distribution variances quantifies the packing of the monolayer for methyl- and hydroxyl-terminated *n*-alkanethiols. The tilt angle distribution for methyl-terminated *n*-alkanethiols is shown in Supporting Information, Figure S1. The peak width for methyl-terminated *n*-alkanethiols follows the same trend with chain length as the distribution for hydroxyl-terminated *n*-alkanethiols.

It should be noted, however, that in Figure 3 we see a non monotonic decrease in tilt angle with decreasing chain length with n=26 showing a shift in the other direction. Figure S1 shows a linear decrease in tilt angle with chain length for methyl-terminated *n*-alkanethiols. This anomalous behavior for hydroxyl terminated *n*-alkanethiols is due to competing interactions of network formation and adlayer mobility which are absent for methyl terminated *n*-alkanethiols.

Further, by quantifying the variance in width of the distribution profile we observe a change of up to five times for hydroxyl-terminated and seven times for methyl-terminated *n*-alkanethiols from n=14→30. Higher chain length exhibits better packing, which has been observed experimentally.[35,36]

The hydrogen-bonded network is stable to wetting and annealing cycles. Compact packing, through increases in chain length and distortion of monolayer assembly through heating cycles (annealing) and contact with water (wetting), can both be observed through changes in the tilt angle distribution profile. The effect of annealing and wetting on S-O tilt angle distribution for chain length n=30 is shown in Figure 4. The symmetric double peaks in S-O tilt angle distribution return to their original shape upon both heating and wetting. The *unidirectional seesaw* network has added stability because it is akin to a frozen layer with directionality. Shifts in tilt angle distributions are a measure of how distorted this network becomes upon perturbation. The

loss in entropy due to increased ordering is balanced through enthalpy release from hydrogen bond formations. Changes in the perturbed state can be seen in the tilt angle distribution. The distribution acts as a quantifier of the degree of disorder in the network. It goes from a split peak to a single peak with loss of the second peak to a shoulder upon wetting (Figure 4A), or a systematic translation to the left upon heating (Figure 4B). A systematic translation to the left is also seen in the S-C tilt angle distribution for hydroxyl-terminated *n*-alkanethiols (Supporting Information Figure S2). The variance in S-O tilt angle distribution with temperature would be a result of variance in end-group orientation and affect dipole moments[37] and spectra.[37,38] IR intensity computed as the square of the changes in dipole moment would change with tilt angles and their dynamic nature with temperature distribution has been observed by Forster-Tonigold *et al.* for benzylmercaptan assembly on Au {111} through a combined vibrational spectroscopy and *ab initio* molecular dynamics (AIMD) approach.[37] The variance in tilt angle distribution in the bezylmercaptan study was seen to increase with temperature and the effects of temperature change were seen as crucial for comparison of measured (IR) and calculated (AIMD) spectra. Sum Frequency Generation (SFG) spectroscopy also quantified changes in tilt angle through changes in the conformation of the terminal group.[38] These studies show that tilt angle is a sensitive quantifier that needs careful choice of characterization methods.

The morphology and structure of hydrogen-bonded networks have been observed through spectroscopic measurements to be two-dimensional (example: oligo(ethylene glycol)) or three-dimensional (example: polyglycine II) depending on the coordination between functional groups that also contributes to the in-plane stability of the monolayers.[39-44] The interplay between hydrogen-bonded network and the odd-even effect has been utilized for photoswitching and biomimetic applications.[45]
The hydroxyl terminated *n*-alkanethiol top network seems to be stable and recoverable towards wetting and annealing, and the trends in tilt angle are best picked by the S-O vector. Changes in external stimuli change the distribution which also changes the population profile, examined in the next section as we establish the *epitaxial transfer* correlates.

Network Transfer

Slopes of variance of the first nearest-neighbor peaks of the radial distribution for the top network atoms (here, O for hydroxyl-terminated and C for methyl-terminated) of the monolayer versus the variance of the adatom (here, S) show a correlation that can be viewed as *epitaxial transfer*. We take variance in radial distribution for S-S versus O-O for hydroxyl-terminated and S-S versus C-C for methyl-terminated *n*-alkanethiols to quantify epitaxial transfer from the top network to the buried adatom gold-sulfur interface (Supporting Information Section S5 has details on computation of epitaxial transfer as variance in peaks of S-S versus O-O or C-C). The correlation in dynamics of the top and bottom layer quantified as the variance in radial distribution function gives a good measure of the cooperative dynamics of the two layers. Shorter spacer length and higher end-group coordination lead to higher network transfer. For n=14 hydroxyl-terminated spacer the epitaxial transfer is ~13.5 times compared to n=30 methyl-terminated *n*-alkanethiol (Figure 5A). The obvious question arises as to the mechanism of the transfer of the top network, or why there would be a correlation between the top network and adatom interface? One possibility would be transfer through chain twist which could lend epitaxy of the top network to the bottom interface. However, the torsional analysis presented in Figure 5B shows that defects do not translate beyond the first methylene group. This means epitaxial transfer should happen through translation of the chain which is seen in mobility and atop percentage values changing with chain length (Figure 6).

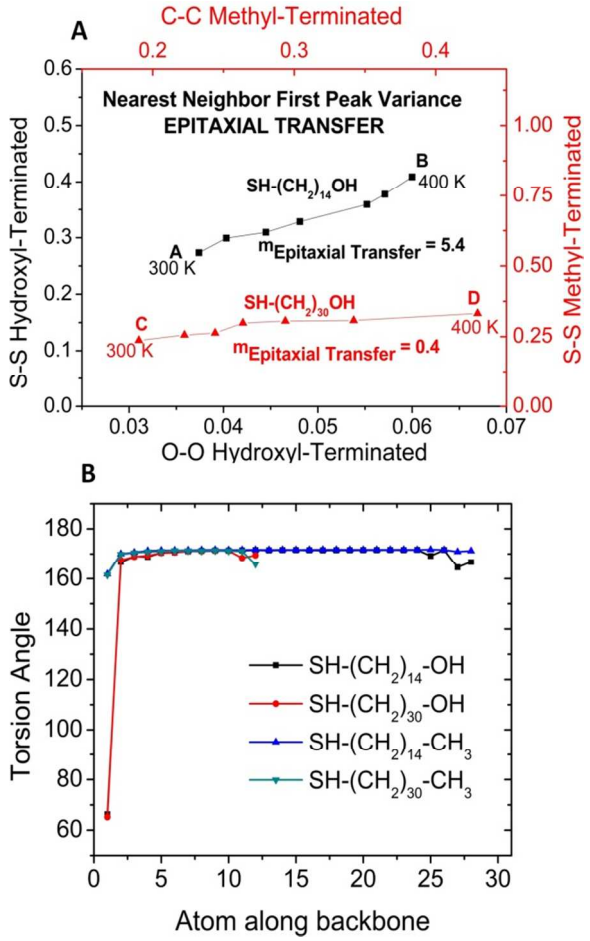

Figure 5: A) Epitaxial transfer shown for two extreme cases of n=14 hydroxyl-terminated and n=30 methyl-terminated *n*-alkanethiol showing the maximum and minimum transfer cases. Short spacer length with a network (n=14, hydroxyl-terminated) favors epitaxial transfer, whereas long spacer lengths with no network (n=30, methyl-terminated) exhibits very little epitaxial transfer. Error in values (variance of the first peak of radial distribution) are ±0.003 based on bin size and averaging. B) Torsion along the backbone as a function of the atom position along the backbone, beginning with the end-group. Two planes are defined four atoms at a time (1,2,3 and 2,3,4) with the first atom being the end-group (O of hydroxyl or C of methyl) and then traveling along the backbone till we reach one carbon above the sulfur. Torsion starts around 60^0 for the first two planes, but quickly increases to 180^0 for all chain lengths (small and large

chain lengths shown) for the two systems, showing lack of defects beyond the first methylene group. The error in values, averaged over a minimum of 500 snapshots, is ±0.1°.

The stability of the monolayer has been observed as increasing as a function of chain length. This was also seen through experimental evidence on stability, packing, and contact angles of *n*-alkanethiol organic layers with increasing chain length.[35,36] We observe a decrease in hopping frequency of the sulfur quantified as decrease in atop percentage with increasing chain length. The network strength also increases with a corresponding increase in the number of hydrogen bonds per oxygen atom. Figure 6 shows that the epitaxial transfer through chain translation leads to better packing and there is competition between the top network transfer, van der Waals interactions and the adatom distribution profile which contribute to the character of the final assembly for a given chain length at a given temperature. In all observations of mobility, packing, network strength, and epitaxial transfer, there is a transition at spacer length near n=24-27. This transition, which would differ for differing backbones and end-groups, could be a design principle for actuation when selecting spacer length based on network and torsion characteristic.

Heating and cooling cycles also result in transitions from hollow to bridge sites, since sampling of the adsorption sites is increased with energy given to the system and the spatially more favorable sites would be available as compared to the thermodynamically more stable sites at lower temperatures. Table 1 shows the effect of annealing on binding-site population for SH-$(CH_2)_{30}$-OH. The bridge-site percentage population at 400 K is preserved upon cooling the monolayer to 300 K. This shows that network transfer is a possibility through annealing, as the system drives toward higher sampling in terms of adatom profile. The higher atop percentage at 400 K is a measure of the hopping of sulfur from hollow to bridge sites. Lower atop percentage upon cooling, when compared to the original monolayer assembly at 300 K, is a measure of overall minimization in adatom energy profile, since atop sites are ~0.3 kcal/mol less favorable energetically (Supporting Information, Tables S1 and S2 for energies of different binding sites) .

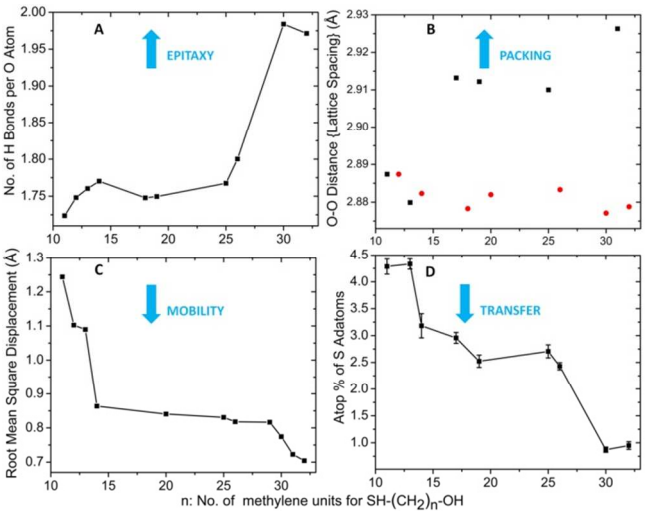

Figure 6: Effect of chain length on epitaxy, packing, mobility, and transfer for hydroxyl-terminated *n*-alkanethiols. Errors for A-C are within the symbol size, the averages being over a minimum of 500 snapshots for 168 chains. Maximum errors have been mentioned in the caption for A-C and plotted for case D. A) Shows that the network strength increases with chain length, leading to higher ability to transfer epitaxy with increasing chain length. The maximum error is ±0.0004. B) Shows that the O-O distance between odd (circle symbol) and even (square symbol) is clearly distinct. The differential slightly increases for higher chain lengths. The maximum error is ±0.0006Å. C) Shows three distinct regions for mobility of the *n*-alkanethiols, with chains below n=14 being highly mobile, followed by a plateau and then a dip for chains approximately greater than n=26. For all graphs, we see a transition around n=24-27 in terms of structural characteristics. The maximum error is ±0.009Å.D) Shows that the population of the atop percentage decreases with increasing chain length. This is in line with the increasing stability of the monolayers with chain length. The shape of S-O tilt angle distribution can be used as a quantifier or a correlate to the adatom population to measure stability of packing.

Table 1. Effect of annealing on binding site population

T(K)	System	Atop %	Bridge %	Hollow %
300	Initial equilibrated	0.87 ± 0.05	56.12 ± 0.25	43.01 ± 0.25
400	Step heated	1.80 ± 0.13	57.12 ± 0.44	41.08 ± 0.44
300	Step cooled	0.58 ± 0.06	57.11 ± 0.33	42.31 ± 0.33

Figure 6A shows the strength of the network, quantified as the number of hydrogen atoms participating per oxygen in the network as increasing with increasing chain length. For a given chain length, if the network is stronger, it has more potential to transfer its pattern (increased epitaxy) to the bottom layer through cooperative packing and dynamics. However, the spacer length and mobility would modulate this transfer of top pattern/induced packing. We also observe a slight decrease in the value of number of hydrogen bonds per oxygen after n=30. This could be due to saturation near n=30, where the network reaches near perfect strength with 1.98 hydrogen bonds. Repulsion due to backbone contributes beyond this perfect network over and above the maximum attraction that the hydrogen bonding can provide. Hence there is low frustration in the network, and we visually observe this, too, in trajectories wherein the best network is for n=30 and there are very small defects for n=32. The saturation also can be seen in Figure S8B in Supporting Information where the average values of non bond energy per methylene unit are plotted as a function of chain length. A minima was seen for n=30, suggesting a near saturation. Moves away from the minima would lead to local frustration in packing and the top network. Figure 6B shows the effect of odd and even chain length on the lattice spacing (O-O distance marked in Figure 2B). For n<14 the lattice spacing does not show a differential because the network is not strong. On average the lattice spacing is 0.04±0.01 Å higher for odd chain lengths, which may mean that the network is able to spread itself and be flexible over a larger space. These effects are well known,[3] and the hydrogen-bonded network modulates -- and weakens to some extent -- the nature of the twist of the end-group. The twist contributes mainly to the increased exposure of

underlying groups of the *n*-alkanethiols. Consistent with prior observations, energies[46] decrease as a function of chain length, which is correlated to packing and may contribute to the change in monolayer properties with chain length.[35,47,48] Hydroxyl-terminated monolayers have lower energy compared to methyl-terminated monolayers (Supporting Information, Section S6 Figure S8 shows energies with chain length variation for both hydroxyl- and methyl-terminated *n*-alkanethiols) which agrees well with our hypothesis that the added stability due to the hydrogen-bonded network is epitaxially transferred to the adatom layer, leading to overall higher stability and better packing. Figure 6C shows the mobility decreasing sharply (Supporting Information Section S7 for details on computation of root mean square displacement), flattening off, and then again decreasing sharply for chain lengths ~n>25. The transfer of the top pattern is aided by shorter spacer lengths, which are more mobile and tend to lead to easier displacement of the chains. Figure 6D shows the decrease in atop percentage, indicating a move towards more energetically favored assemblies, as atop binding sites are ~0.3 kcal/mol higher in energies. The saturation effect observed in 6A is also seen to some extent in 6D, where the atop % flattens out instead of going down. The value of atop % for n =30 is extremely small (as shown in Table I). Therefore, hopping after n=30 may stabilize because the absolute values are quite small and stabilization beyond this point may not be realizable.

In summary, quantification through split-peak characteristics of the S-O tilt angle vector distribution for hydroxyl-terminated *n*-alkanethiols are a measure of modulation of the hydrogen-bonded network with monolayer packing. Top network characteristics, when coupled with the variance in adatom profile and population analyses of the adsorption sites, provide measures of *epitaxial transfer* which could be useful tools for monolayer assembly design principles. The competing factors of hydrogen bonding of the end functional groups and their interplay with backbone odd-even packing effects have been utilized for the synthesis of a number of functional materials, from photoswitchable surfaces[11] to van der Waals rectifiers.[4,5] The quantification methods proposed offer insight into the exact contribution of each effect as a function of chain length. Modulation of the top network through annealing and wetting, and changes in epitaxial transfer to the buried gold-sulfur interface through changes in spacer length have been observed. Tuning the inherent odd-even effects through additional network formation by end-group coordination provides increased control over twist of the end-group. These trends and quantifiers could be used for rational design of polymer-based nanoactuators[49,50] that depend on torsional changes in the backbone, or biosensors[10] that in turn depend on exact knowledge of binding-site profiles.[51,52]

Acknowledgments

We are grateful to Prof. Ali Dhinojwala for pointing out the spectral information available for the hydrogen bond network in different monolayer assemblies and for general comments on the paper; Prof. Hendrik Heinz for comments on soft epitaxy, sulfur interaction with gold, and fcc metal potentials; Dr. Selemon Bekele for help with distribution plots of hydrogen bonding utilizing the Root software and Gary Leuty and He Zhu for useful comments on the paper and general discussions. This work was supported by National Science Foundation (NSF) grant DMR0847580.

References

1 P.E. Laibinis, G. W. Whitesides and D. L. Allara, *J. Am. Chem. Soc.* **1991**, 113, 7152.
2 K. Edinger, A. Goelzhaeuser, K. Demota, C. Woell and M. Grunze, *Langmuir* **1993**, 9, 4.
3 F. Tao, F. T. Bernasek, *Chem. Rev.* **2007**, 107, 1408.
4 F. T. Bernasek, *Nature Nanotech.* **2013**, 8, 80.
5 N. Nerngchamnong, L. Yuan, D-C. Qi, J. Li, D. Thompson and C. A. Nijhuis, *Nature Nanotech.* **2013**, 8, 113.
6 L. Venkataraman, J. E. Klare, C. Nuckolls, M. S. Hybertsen and M. L. Steigerwald, *Nature* **2006**, 442, 904.
7 D. Q. Andrews, R. P. van Duyne and M. A. Ratner, *Nano Lett.* **2008**, 8, 1120.
8 G. Foti, D. Sánchez-Portal, A. Arnau and T. Frederiksen, *J. Phys. Chem. C* **2013**, 117, 14272.
9 L. Venkataraman, J. E. Klare, I. W. Tam, C. Nuckolls, M. S. Hybertsen and M. L. Steigerwald, *Nano Lett.* **2006**, 6, 458.
10 N. K. Chaki and K. Vijayamohanan, *Biosensors and Bioelectronics* **2002**, 17, 1.
11 A. S. Kumar, T. Ye, T. Takami, B. C. Yu, A. K. Flatt, J. M. Tour and P. S. Weiss, *Nano Lett.* **2008**, 8, 1644.
12 Y. Selzer, L. Cai, M. A. Cabassi, Y. Yao, J. M. Tour, T. S. Mayer and D. L. Allara, *Nano Lett.* **2005**, 5, 61.
13 S. Griessl, M. Lackinger,M. Edelwirth, M. Hietschold and W. M. Heckl, *Single Molecules* **2002**, 3, 25.
14 M. Yu, N. Bovet,C. J. Satterley, S. Bengió, K. R. J. Lovelock, P. K. Milligan, R. G. Jones, D. P. Woodruff and V. Dhanak, *Phys. Rev. Lett.* **2006**, 97, 166102.
15 M. Tachibana, K. Yoshizawa, A. Ogawa, H. Fujimoto and R. Hoffmann, *J. Phys. Chem. B* **2002**, 106, 12727.
16 F. Chen, X. Li, J. Hihath, Z. Huang and N. Tao, *J. Am. Chem. Soc.* **2006**, 128, 15874.
17 R. S. Clegg and J. E. Hutchison, *J. Am. Chem. Soc.* **1999**, 121, 5319.
18 H. Wolf, H. Ringsdorf, E. Delamarche, T. Takami, H. Kang, B. Michel, C. Gerber, M. Jaschke, H.-J. Butt and E. Bamberg, *J. Phys. Chem.* **1995**, 99, 7102.
19 T. Elzein, A. Fahs, M. Brogly, A. Elhiri, B. Lepoittevin, P. Roger and V. Planchot, *J. Adhesion* **2013**, 89, 416.
20 L. Newton, T. Slater, N. Clark and A. Vijayaraghavan, *J. Mater. Chem. C* **2013**, 1, 376.
21 F. Li, L. Tang, W. Zhou and Q. Guo, *J. Am. Chem. Soc.* **2010**, 132, 13059.
22 C. Vericat, M. E. Vela and R. C. Salvarezza, *Phys. Chem. Chem. Phys.* **2005**, 7, 3258.
23 C. Vericat, M. E. Vela, G. A. Benitez, J. M. Gago, X. Torrelles and R. C. Salvarezza, *J. Phys.: Condens. Matter* **2006**, 18, R867.
24 J. Zhao and K. Uosaki, *Nano Lett.* **2002**, 2, 137.
25 S. O'Mahony, C. O'Dwyer, C. A. Nijhuis, J. C. Greer, A. J. Quinn and D. Thompson, *Langmuir* **2013**, 29, 7271.
26 H. Heinz, R. A. Vaia, B. L. Farmer and R. R. Naik, *J. Phys. Chem. C* **2008**, 112, 17281.
27 W. L. Jorgensen and J. Tirado-Rives, *J. Am. Chem. Soc.* **1988**, 110, 1657.
28 J. Feng, R. B. Pandey, R. J. Berry, B. L. Farmer, R. R. Naik and H. Heinz, *Soft Matter* **2011**, 7, 2113-2120
29 J. Feng, J. M. Slocik, M. Sarikaya, R. R. Naik, B. L. Farmer and H. Heinz, *Small* **2012**, 8, 1049.
30 W. Mar and M. L. Klein, *Langmuir* **1994**, 10, 188.
31 R. Godawat, S. N. Jamadagni and S. P. Garde, *Proc. Natl. Acad. Sci. USA* **2009**, 106, 15119.
32 L. Strong and G. M. Whitesides, *Langmuir* **1988**, 4, 546.
33 A. Cossaro, R. Mazzarello, R. Rousseau, L. Casalis, A. Verdini, A. Kohlmeyer and G. Scoles, *Science* **2008**, 321, 943.
34 A. Gavezzotti and G. Filippini, *J. Phys. Chem.* **1994**, 98, 4831.

35 M. D. Porter, T. B. Bright, D. L. Allara and C. E. Chidsey, *J. Am. Chem. Soc.* **1987**, 109, 3559.
36 L. Srisombat, A. C. Jamison and T. R. Lee *Colloids Surf. A* **2011**, 390, 1.
37 K. Forster-Tonigold, X. Stammer, C. Wöll and A. Groß, *Phys. Rev. Lett.* **2013**, 111, 086102.
38 P. J. N. Kett, M. T. L. Casford and P. B. Davies, *J. Phys. Chem. Lett.*, **2012**, 3, 3276.
39 R. Valiokas, S. Svedhem, S. C. Svensson and B. Liedberg, *Langmuir* **1999**, 15, 3390.
40 S. W. Tam-Chang, H. A. Biebuyck, G. M. Whitesides, N. Jeon and R. G. Nuzzo, *Langmuir* **1995**, 11, 4371.
41 R. C. Sabapathy, S. Bhattacharyya, M.C. Leavy, W. E. Cleland and C. L. Hussey, *Langmuir* **1998**, 14, 124.
42 R. S. Clegg and J. E. Hutchison, *Langmuir* **1996**, 12, 5239.
43 T. J. Lenk, V. M. Hallmark, C. L. Hoffmann, J. F. Rabolt, D. G. Castner, C. Erdelen and H. Ringsdorf, *Langmuir* **1994**, 10, 4610.
44 R. S. Clegg, S. M. Reed and J. E. Hutchison, *J. Am. Chem. Soc.* **1998**, 120, 2486.
45 X. Liu, T. Wang and M. Liu, *Langmuir* **2012**, 28, 3474.
46 E. Torres, A. T. Blumenau, and P. U. Biedermann, *ChemPhysChem* **2011**, 12, 999.
47 X. Cai and S. Baldelli, *J. Phys. Chem. C* **2011**, 115, 19178.
48 S. Malkhandi, B. Yang, A. K. Manohar, G. S. Prakash and S. R. Narayanan, *J. Am. Chem. Soc.* **2012**, 135, 347.
49 S. Zou, M. A. Hempenius, H. Schönherr and G. J. Vancso *Macromol. Rapid Comm.* **2006**, 27, 103.
50 W. Shi, M. I. Giannotti, X. Zhang, M. A. Hempenius, H. Schönherr and G. J. Vancso, *Angew. Chem. Int. Ed.* **2007**, 46, 8400.
51 Z. Matharu, A. J. Bandodkar, V. Gupta and B. D. Malhotra, *Chem. Soc. Rev.* **2012**, 41, 1363.
52 J. R. Heath, *Annu. Rev. Mater. Res.* **2009**, 39, 1.